Scalable Electro-Optic Control of Localized Bistable Switching in Broad-Area VCSELs Using Reconfigurable Funnel Waveguides

R. Martínez-Lorente,[1,2] J. Parravicini,[3] M. Brambilla,[4] L. Columbo,[5,6] F. Prati,[7] C. Rizza,[8] A. J. Agranat,[9] and E. DelRe[2,*]

[1]*Departamento de Óptica y Optometría y Ciencias de la visión, Universitat de València, 46010 València, Spain*

[2]*Dipartimento di Fisica, Università di Roma "La Sapienza", 00185 Rome, Italy*

[3]*Dipartimento di Scienza dei Materiali and MIB-SOLAR, Università degli Studi di Milano-Bicocca, 20125 Milano, Italy*

[4]*Dipartimento Interateneo di Fisica, Università e Politecnico di Bari, 70126 Bari, Italy*

[5]*CNR-IFN, 70126 Bari, Italy*

[6]*Dipartimento di Elettronica e Telecomunicazioni, Politecnico di Torino, 10129 Torino, Italy*

[7]*Dipartimento di Scienza & Alta Tecnologia, Università dell'Insubria, 22100 Como, Italy*

[8]*Department of Industrial and Information Engineering and Economics, University of L'Aquila, 67100 L'Aquila, Italy*

[9]*Applied Physics Department, Hebrew University of Jerusalem, 91904 Jerusalem, Israel*

(Received 10 October 2016; revised manuscript received 21 April 2017; published 6 June 2017)

We demonstrate a steplike optical modulation based on the activation and deactivation of a bistable localized structure using a photoinduced and reconfigurable miniaturized 30×30 μm electroactivated funnel waveguide. Control of a single 10-μm-diameter spot in a 200-μm-diameter vertical-cavity surface-emitting laser at 980 nm is achieved modulating the phase of an exciting beam in the specific position of the spot in the cavity. This localized on-off response can be scaled into arrays and offer a possible route to fast integrated optical logical functions and memory at low intensities at near-infrared wavelengths.

DOI: 10.1103/PhysRevApplied.7.064004

I. INTRODUCTION

Optical modulators do not easily reproduce the response of basic digital electronic circuits, such as the all-important steplike response, rendering even the most elementary building blocks of a "digital" optics, such as optical memories and optical logic gates, a challenge [1–3]. Although remarkable advances have been achieved in integrated optical modulators, especially in silicon photonics for telecommunication wavelengths [4], the search is on for a fast, scalable, and integrated steplike intensity modulator.

One approach is based on the use of bistable systems. In a bistable system, only two states are possible, and the response will be naturally steplike even when the driving signal is not. Dissipative self-localized structures in active cavities offer an enhanced versatility, since each bistable structure can form in, and be moved to, different positions throughout the device cross section, thus yielding an effective spatial multistability for switching. For example, vertical-cavity surface-emitting lasers (VCSELs) with a broad emission area can host bistable localized micrometric structures (LSs) that are externally addressable and able to store and process information. This forms the optical equivalent of a blackboard mapped across a device-dependent patchwork in the active area [5–8]. In this vein, the single LS should be optically addressed using a conventional electro-optic phase modulator while the steplike conversion occurs for the light it emits, a principle that has been demonstrated using a piezoelectric-driven interferometric scheme [9]. In turn, the possibility of extending this control to a full transverse plane has been demonstrated using a liquid-crystal spatial phase mask [10]. Ideally, each LS should be addressable independently and use a fast electro-optic phase modulator, a challenge that requires the miniaturization and integration of fast optical modulators operating in the visible and near infrared. In a recent development, a miniaturized intensity modulator based on an electroactivated waveguide was used to excite a LS [11]. The approach is based on electroactivated circuitry, that is, volume-integrated electro-optic waveguides generated through spatial solitons or optical funnels that are modulated using the quadratic electro-optic effect. These circuits are wholly reconfigurable through photoinduction and can be miniaturized, scaled into arrays [12], fiber coupled [13], and electroactivated with a fast nanosecond response also for visible and near-infrared light [14].

Here, we demonstrate an electrically driven steplike optical modulation in the light emitted by an LS using a miniaturized funnel-waveguide electro-optic phase modulator in a sample of $K_{1-y}Li_yTa_{1-x}Nb_x$ (KLTN) [15–17]. The LS forms in a 200-μm-wide VCSEL kept below threshold emitting at $\lambda = 978$ nm and is locally excited or de-excited by modulating the phase of a focused beam relative to the background holding beam. The phase sweep, which is tuned

*eugenio.delre@uniroma1.it

 © 2017 American Physical Society

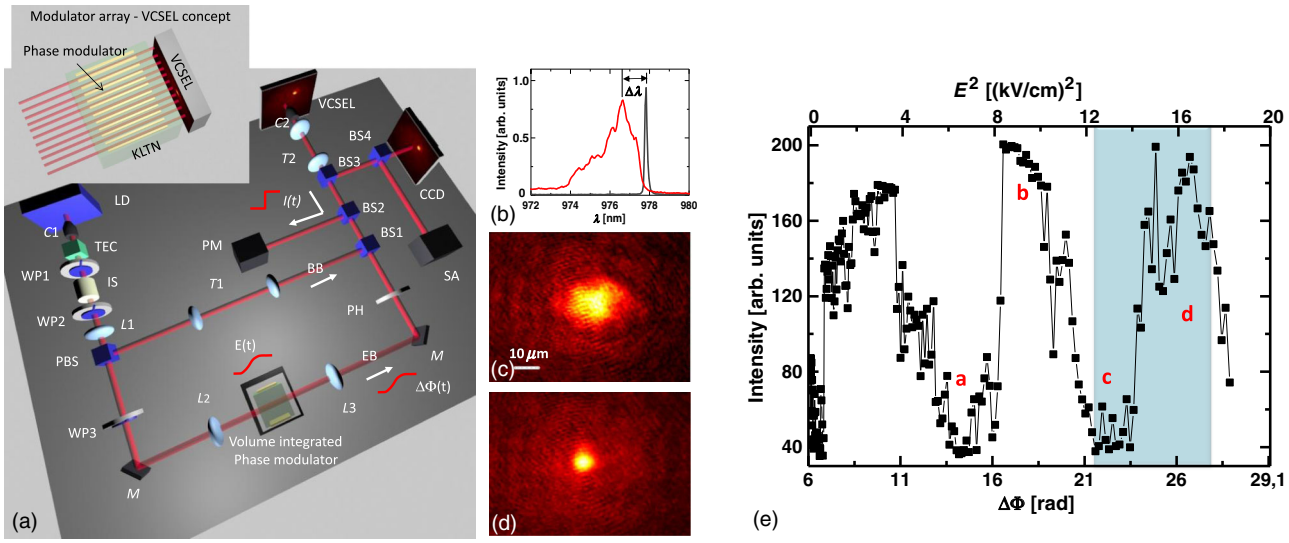

FIG. 1. Demonstrating a steplike response in LS activation or deactivation using a volume-integrated photoinduced miniaturized electro-optic phase modulator. (a) Experimental setup (see text) and applicative concept (inset). (b) Typical broad spectrum of the broad-area VCSEL (red curve) and of the exciting beam (black curve) where $\Delta\lambda$ is the shift between the two peaks in the spectrum. (c) Light emitted by the VCSEL with the BB in proximity of an emission island (the slight asymmetry depends on alignment) and (d) the same region with also the EB, in conditions activating the LS. (e) Optical on-off response: intensity of the LS emission from the VCSEL as a function of the applied electrical field E (see text). The red labels a–d indicate the conditions corresponding to the spatial intensity distributions reported in Fig. 2. The shaded region indicates the data aggregated into Fig. 2(f). Note the asymmetry in the on-off and off-on transitions.

to be slower than the two-state transition time of the LS, accesses the underlying bistability and leads to the on-off and off-on response [11,18]. The result extends previous steplike experiments using bistable localized structures to a configuration that can be integrated into dense arrays and potentially operated at fast nanosecond time scales.

II. EXPERIMENTAL SETUP AND PROCEDURE

The proof of concept of a single miniaturized element is performed using the experimental setup illustrated Fig. 1(a), while the complete scheme of the ideal reconfigurable integrated array is illustrated in the inset. We should note that in the presently available broad-area VCSELs, the regions forming the optical blackboard are a device- and condition-dependent patchwork that spans the active area. A laser beam (red beam) is split into a background beam (BB) and exciting beam (EB). As the EB propagates through the biased funnel-waveguide modulator, its phase suffers a shift $\Delta\Phi(t)$ caused by the applied electric field $E(t)$. As the EB recombines with the BB and is coupled into a VCSEL, light is emitted and manifests a steplike signature in the corresponding $I(t)$.

In detail, an infrared laser beam from a semiconductor laser diode (LD, $\lambda \simeq 978$ nm, 200–400 mW optical power emission, spectral range of 15 nm) is collimated ($C1$) and filtered by a tunable Littman-Metcalf cavity (TEC). It passes through a pair of $\lambda/2$ wave plates (WP1/2), an optical isolator (IS), and a launch lens $L1$ before being split into the BB and EB by a polarizing beam splitter (PBS). In combination with the wave plates, this allows the balancing of the relative BB and EB beam powers. The polarization of the EB is once again rotated to be parallel to that of the BB by WP3 and lenses $L2$ and $L3$ couple into and out of a funnel waveguide imprinted in a sample of photorefractive KLTN (PR). The waveguide has been previously prepared using a CW visible laser beam ($\lambda = 532$ nm, $\simeq 20$ mW) following the procedure described elsewhere [11,16,17], and the PR is biased by an electric field E that introduces a shift in the phase of EB relative to BB ($\Delta\Phi$) [15]. The BB passes through the beam expander $T1$ and is recombined to the EB at BS1. A final beam expander $T2$ and collimator $C2$ injects both EB and BB into the 200-μm VCSEL. The surface of the VCSEL is inspected using a spectrum analyzer (SA), a CCD camera (CCD), and a power meter (PM) [6,11,19,20]. An iris pin-hole (PH) is placed after the PR to obtain a homogeneous EB [15]. The detuning $\Delta\lambda$ between the injected beam and the VCSEL emission peak (when brought above threshold) is fixed changing the wavelength of the EB through the TEC and the VCSEL temperature [Fig. 1(b)].

In our specific batch of VCSELs (ULM Photonics, 980-00-TN-H56 OOP), optically injected LSs form when the current is tuned in the range 75–200 mA and the temperature in the range 22–26 °C. Regions in the active area are selected with defects that allow the spontaneous formation of stable and fixed regions of increased emission even with no EB [19,21,22]. The wavelength detuning $\Delta\lambda$ between the VCSEL emission and the BB (measured at the peaks of the spectra) is then continuously changed. In a range of $\Delta\lambda$ from $\simeq$1.01 to $\simeq$1.07 nm there are a variable number of

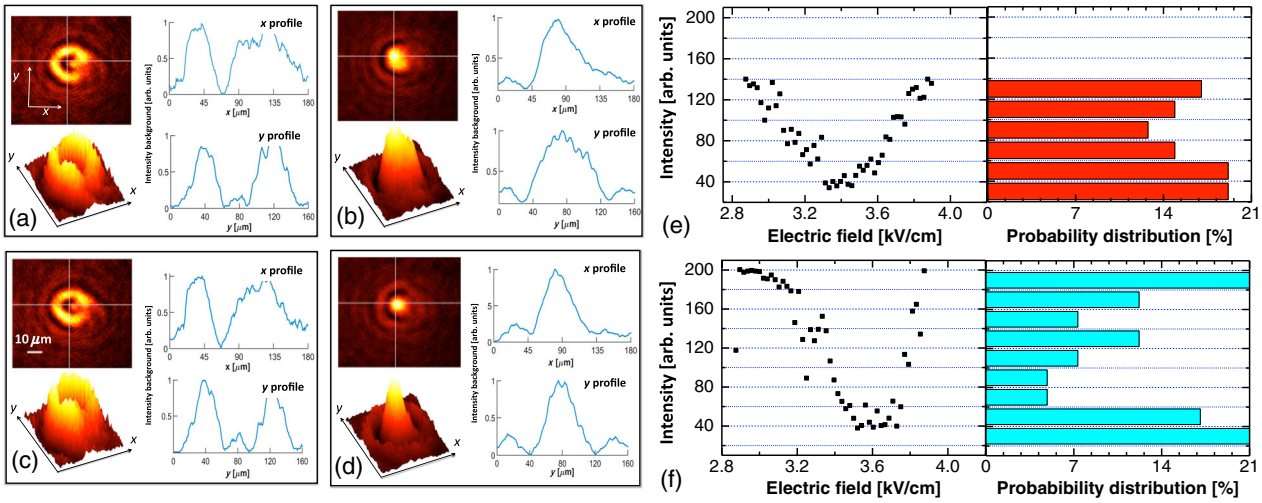

FIG. 2. Transverse intensity distributions and x and y profiles (background is subtracted for added clarity) of the emitted light for different values of E and $\Delta\Phi$: (a) 2.58 kV/cm and 14.34 rad (deactivation), (b) 3.13 kV/cm and 18.29 rad (activation), (c) 3.66 kV/cm and 22.98 rad (deactivation), and (d) 4.04 kV/cm and 26.06 rad (activation). Note the phase-dependent ringlike structures. (e) (left) intensity versus E and (right) data histogram in conditions not leading to the formation of LSs ($\Delta\lambda \neq 1.18$ nm) compared to (f) same data in conditions leading to LS activation or deactivation.

islands (generally from 1 to 5) of enhanced emission [see Fig. 1(c)], each amounting to about $1/7$ of the total device area, in which bistable LS can form. In the inspected cases we find no clear evidence of island cross talk. The island size and distribution, that are both device and condition dependent, ultimately fix, in our experiment, the minimum distance between independent LS to 35 μm and the maximum number of LS to 5. LS formation is found also to depend on $\Delta\lambda$, mutual VCSEL-BB alignment, and the intensity of the BB. After the identification of the suitable regions, the increased emission in proximity of cavity defects are switched off by increasing $\Delta\lambda$. The EB is then injected into the VCSEL. The BB and EB have approximately the same intensity ($P_{\mathrm{BB}} \simeq 3.3$ mW, $P_{\mathrm{EB}} \simeq 15.9$ μW). The EB is launched in the proximity of a defect supporting a region of enhanced emission and the detuning is increased to $\Delta\lambda \simeq 1.18$ nm. The activation and deactivation experiments are carried out with $\lambda_{\mathrm{EB}} = 977.83$ nm and $\lambda_{\mathrm{VCSEL}} = 976.65$ nm, $\mathrm{T_{VCSEL}} = 26.43\,^{\circ}\mathrm{C}$ and $\mathrm{I_{VCSEL}} = 128.06$ mA. The relative phase between EB and BB is then changed by appropriately changing the voltage applied to the funnel-waveguide modulator [15]. An activated LS is reported in Fig. 1(d), and activation occurs with up to a 20-μm misalignment between the EB and the defect.

III. RESULTS AND COMPARISON TO MODEL

In Fig. 1(e) we report the LS activation and deactivation as a function of the electric field E applied to the electro-optical funnel waveguide and associated phase shift $\Delta\Phi$. The intensity I is measured in the central region of the LS [Fig. 1(d)]. The transverse x, y intensity distribution for different stages in the modulation are reported in Figs. 2(a)–2(d)]. The on-off response is further detailed comparing the emitted intensity versus E in conditions not leading to LS [Fig. 2(e)] to those leading to LS [Fig. 2(f)]. Histograms of the data indicate that, as bistability sets in, the LS is activated and deactivated abruptly, without passing through intermediate values of emitted intensity.

The steplike response of Fig. 1, with an on-off extinction ratio of 5, confirms previous steplike experiments and can be interpreted through simulations based on the well-established model of VCSEL spatiotemporal dynamics [6,23]. Specifically, we adopt the model equations (8a) and (8b) of [24] and the laser parameters relative to Fig. 8 therein, a condition compatible with our present experiments.

The input field Y is modeled by superimposing a plane-wave background beam (BB) and a narrow pulse acting as an exciting beam (EB), whose phase is linearly varied in $(0, 2\pi)$ throughout the simulations. The variation is carried out so as to ensure that the field is adiabatically always at steady state. Assuming

$$Y(t) = Y_{\mathrm{BB}} + Y_{\mathrm{EB}} \exp\left[-(x^2 + y^2)/(2\sigma^2)\right] \exp[i\phi(t)], \quad (1)$$

we choose $Y_{\mathrm{BB}} = 0.75$ to ensure that the laser is in a regime where LSs, similar to those described previously, and identified as cavity solitons (CS) are stable [see Fig. 8(a) in [24]] and $Y_{\mathrm{BB}} = Y_{\mathrm{EB}}$ to meet the experimental conditions. The width of the EB is chosen comparable to the CS diameter. We consider an initial condition where a steady-state CS is present on the optical axis and evaluate the field intensity at this location while the phase is varied in $(0, 2\pi)$ (black line) and back (red line). Figure 3 shows the plot of the predicted intensity versus phase, where one can appreciate the CS switching off and on as the phase variation causes the EB and

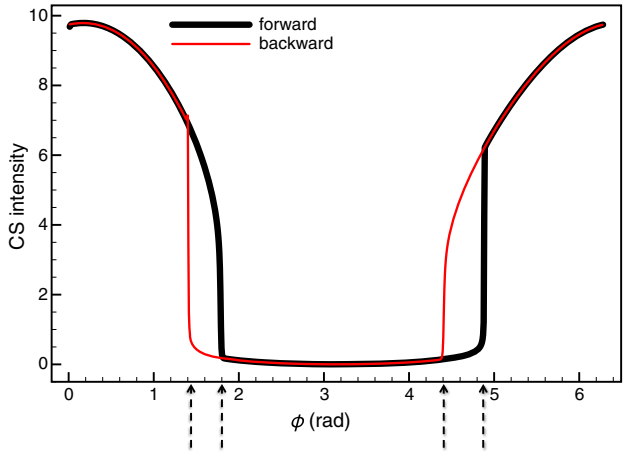

FIG. 3. Simulation results of the intensity at optical axis versus EB phase during an adiabatic phase sweep from 0 to 2π (black line) and back (red line). The dashed arrows mark hysteresis regions. For the purpose of interpreting our experiments, this hysteresis leaves the fingerprint in the form of an asymmetry in the rise and fall sections of the signal [see Fig. 2(f)].

the BB to interfere destructively and constructively, respectively. Note the coexistence of the on and off states which indicates a bistability between the homogeneous state and the CS branch (as seen in Fig. 8 of [24]) and the asymmetry in the switch-off and switch-on processes as observed in the experiment (Fig. 2). The bistability is evidenced by arrows in Fig. 3.

The ringlike structures observed in the transverse intensity distributions of Fig. 2 suggest a residual phase profile in the EB from the miniaturized modulator described in [15,25]. This is confirmed by simulations, further indicating the existence of an area around the LS reasonably free of defects and emission anomalies. The effect can be simulated in the model by assuming an EB phase that presents a transverse Gaussian spatial modulation, compounded with the time-varying phase introduced previously. We consider thus

$$\phi(x,y,t) = \varphi(t) + \delta\phi \exp\left[-(x^2+y^2)/(2\xi^2)\right], \quad (2)$$

where $\delta\phi$ is taken constant while $\varphi(t)$ is varied during the simulation in the range $(0, 8\pi)$ forward and backward; ξ is larger than σ and compatible with the size of the funnel waveguide at the VCSEL plane ($\sigma/\xi \simeq 3/5$ in our simulations). This phase replaces $\phi(t)$ in Eq. (1) and allows the simulation of a spatially distributed phase interference between a plane-wave BB and a complex, time varying EB.

The visualizations Visualization1.avi and Visualization2.avi provided as Supplemental Material [26] show the temporal evolution of the intracavity field profile as the phase is varied forward and backward, respectively. Specific results are presented for $Y_{\mathrm{BB}} = 0.5$ and $Y_{\mathrm{EB}} = 0.7$. The formation and alternation of rings that accompany the onset and erasure of the central CS are in agreement with the experiments.

Our experiments drive an LS using a miniaturized funnel waveguide at steady state. The actual time response of the assembly depends on the specific details of the two underlying components, i.e., the electro-optic response of KLTN τ_1 and the activation and deactivation time in the VCSEL τ_2. Although τ_1 can potentially be below the nanosecond time scale using traveling-wave radio-frequency techniques, standard electric driving of KLTN leads to a $\tau_1 \sim 10$ ns [14]. In turn, τ_2 is determined by the excitation-recombination process in the active medium and in conditions comparable to ours has been measured to be $\tau_2 \sim 5$ ns [9].

IV. CONCLUSIONS

We demonstrate the activation and deactivation of localized light structures in a broad-area VCSELs by employing a phase modulator based on an electro-optical funnel waveguide with a potential nanosecond response and micrometric transverse miniaturization [14]. Our results expand previous findings on steplike two-state response using bistability [8,9] demonstrating miniaturized electro-optic control that can be potentially scaled into dense arrays and driven to speeds typical of cutting-edge optical modulation technology. While this builds on previous results, introducing no conceptual modifications in our understanding of the underlying soliton physics, it opens alternative applicative scenarios in optical information processing and optical memories, and a similar configuration can be developed to implement optical logical gates (AND, OR, NAND, and NOR) [27]. Future progress is required to deploy a full-fledged array of modulators, butt couple the modulators to the VCSEL, and evaluate response time, long-term stability, and overall complexity of the assembly compared to presently deployed interferometric modulation techniques.

ACKNOWLEDGMENTS

Funding from La Sapienza (Ricerca di Ateneo 2016) is acknowledged.

[1] E. Kuramochi, K. Nozaki, A. Shinya, K. Takeda, T. Sato, S. Matsuo, H. Taniyama, H. Sumikura, and M. Notomi, Large-scale integration of wavelength-addressable all-optical memories on a photonic crystal chip, Nat. Photonics **8**, 474 (2014).

[2] M. R. Sprague, P. S. Michelberger, T. F. M. Champion, D. G. England, J. Nunn, X.-M. Jin, W. S. Kolthammer, A. Abdolvand, P. St. J. Russell, and I. A. Walmsley, Broadband single-photon-level memory in a hollow-core photonic crystal fibre, Nat. Photonics **8**, 287 (2014).

[3] C. Ros, M. Stegmaier, P. Hosseini, D. Wang, T. Scherer, C. D. Wright, H. Bhaskaran, and W. H. P. Pernice, Integrated all-photonic non-volatile multi-level memory, Nat. Photonics **9**, 725 (2015).

[4] G. T. Reed, G. Mashanovich, F. Y. Gardes, and D. J. Thomson, Silicon optical modulators, Nat. Photonics **4**, 518 (2010).

[5] T. Ackemann, W. Firth, and G. L. Oppo, Fundamentals and applications of spatial dissipative solitons in photonic devices, Adv. At. Mol. Opt. Phys. **57**, 323 (2009).

[6] S. Barland, J. R. Tredicce, M. Brambilla, L. Lugiato, S. Balle, M. Giudici, T. Maggipinto, L. Spinelli, G. Tissoni, T. Knödl, M. Miller, and R. Jäger, Cavity solitons as pixels in semiconductor microcavities, Nature (London) **419**, 699 (2002).

[7] M. Marconi, J. Javaloyes, S. Barland, S. Balle, and M. Giudici, Vectorial dissipative solitons in vertical-cavity surface-emitting lasers with delays, Nat. Photonics **9**, 450 (2015).

[8] X. Hachair, L. Furfaro, J. Javaloyes, M. Giudici, S. Balle, J. Tredicce, G. Tissoni, L. A. Lugiato, M. Brambilla, and T. Maggipinto, Cavity solitons switching in semiconductor microcavities, Phys. Rev. A **72**, 013815 (2005).

[9] S. Barbay, Y. Mnesguen, X. Hachair, L. Leroy, I. Sagnes, and R. Kuszelewicz, Incoherent and coherent writing and erasure of cavity solitons in an optically pumped semiconductor amplifier, Opt. Lett. **31**, 1504 (2006).

[10] F. Pedaci, P. Genevet, S. Barland, M. Giudici, and J. R. Tredicce, Positioning cavity solitons with a phase mask, Appl. Phys. Lett. **89**, 221111 (2006).

[11] J. Parravicini, M. Brambilla, L. Columbo, F. Prati, C. Rizza, G. Tissoni, A. J. Agranat, and E. DelRe, Observation of electro-activated localized structures in broad area VCSELs, Opt. Express **22**, 30225 (2014).

[12] A. D'Ercole, E. Palange, E. DelRe, A. Ciattoni, B. Crosignani, and A. J. Agranat, Miniaturization and embedding of soliton-based electro-optically addressable photonic arrays, Appl. Phys. Lett. **85**, 2679 (2004).

[13] E. DelRe, E. Palange, and A. J. Agranat, Fiber-launched ultratight photorefractive solitons integrating fast soliton-based beam manipulation circuitry, J. Appl. Phys. **95**, 3822 (2004).

[14] N. Sapiens, A. Weissbrod, and A. J. Agranat, Fast electroholographic switching, Opt. Lett. **34**, 353 (2009).

[15] J. Parravicini, F. Di Mei, R. Martinez Lorente, D. Pierangeli, A. J. Agranat, and E. Del Re, Volume integrated phase-modulator based on funnel waveguides for reconfigurable miniaturized optical circuits, Opt. Lett. **40**, 1386 (2015).

[16] A. Pierangelo, A. Ciattoni, E. Palange, A. J. Agranat, and E. DelRe, Electro-activation and electro-morphing of photorefractive funnel waveguides, Opt. Express **17**, 22659 (2009).

[17] E. DelRe, A. Pierangelo, J. Parravicini, S. Gentilini, and A. J. Agranat, Funnel-based biomimetic volume optics, Opt. Express **20**, 16631 (2012).

[18] L. Columbo, C. Rizza, M. Brambilla, F. Prati, and G. Tissoni, Controlling cavity solitons by means of photorefractive soliton electro-activation, Opt. Lett. **37**, 4696 (2012).

[19] E. Averlant, M. Tlidi, H. Thienpont, T. Ackemann, and K. Panajotov, Experimental observation of localized structures in medium size VCSELs, Opt. Express **22**, 762 (2014).

[20] Y. Tanguy, T. Ackemann, and R. Jäger, Characteristics of switching dynamics in a semiconductor-based cavity-soliton laser, Opt. Express **15**, 16773 (2007).

[21] F. Pedaci, G. Tissoni, S. Barland, M. Giudici, and J. Tredicce, Mapping local defects of extended media using localized structures, Appl. Phys. Lett. **93**, 111104 (2008).

[22] E. Caboche, S. Barland, M. Giudici, J. Tredicce, G. Tissoni, and L. A. Lugiato, Cavity-soliton motion in the presence of device defects, Phys. Rev. A **80**, 053814 (2009).

[23] M. Brambilla, L. A. Lugiato, F. Prati, L. Spinelli, and W. J. Firth, Spatial Soliton Pixels in Semiconductor Devices, Phys. Rev. Lett. **79**, 2042 (1997).

[24] L. Spinelli, G. Tissoni, M. Brambilla, F. Prati, and L. A. Lugiato, Spatial solitons in semiconductor microcavities, Phys. Rev. A **58**, 2542 (1998).

[25] J. Parravicini, F. Di Mei, D. Pierangeli, A. J. Agranat, and E. DelRe, Miniaturized electro-optic infrared beam manipulator based on 3D photorefractive funnels, J. Opt. **17**, 055501 (2015).

[26] See Supplemental Material at http://link.aps.org/supplemental/10.1103/PhysRevApplied.7.064004 for the time evolution of the simulated intracavity field.

[27] L. Columbo, C. Rizza, M. Brambilla, F. Prati, and G. Tissoni, A concomitant and complete set of nonvolatile all-optical logic gates based on hybrid spatial solitons, Opt. Express **22**, 6934 (2014).